

A spectroscopic search for red supergiants in the M33 giant H II region NGC 604

Elena Terlevich,¹ Angeles I. Díaz,² Roberto Terlevich,³ Rosa M^a. González-Delgado,^{4,5★} Enrique Pérez^{4★} and María L. García Vargas^{2†}

¹*Institute of Astronomy, Madingley Road, Cambridge CB3 0HA*

²*Departamento Física Teórica CXI, Universidad Autónoma, Cantoblanco, 28049 Madrid, Spain*

³*Royal Greenwich Observatory, Madingley Road, Cambridge CB3 0EZ*

⁴*Instituto de Astrofísica de Andalucía, Apartado 3004, 18080 Granada, Spain*

⁵*Instituto de Astrofísica de Canarias, Vía Láctea s/n, 38200 La Laguna, Tenerife, Spain*

Accepted 1995 November 3. Received 1995 November 2; in original form 1995 August 31

ABSTRACT

We present high signal-to-noise ratio spectrophotometry obtained in the optical and near-infrared with the double spectrograph ISIS on the WHT, of the M33 giant H II region NGC 604. Our main aim was to deduce global properties of a nearby giant H II region. The near-infrared spectral range, central to our study, comprises the gravity-sensitive Ca II triplet (CaT) stellar absorption features. The data were obtained using two different techniques: (1) scanning with a 1.75-arcmin-long slit that provided integrated spectra of the central part of the nebula, and (2) long-slit spectra of the brightest continuum knots.

A single red supergiant (RSG) star was detected, judging from the measured strength of the stellar CaT absorption lines, visible in one region and only after carefully subtracting the hydrogen Paschen emission lines that dominate the near-infrared spectra. The feature is not observed in the integrated spectrum. The observed Paschen discontinuity in emission allows us to determine an electron temperature, which is similar to the one obtained from the ratio of forbidden line ([O III]) intensities, suggesting that temperature fluctuations are not present in the nebula.

Wolf-Rayet (WR) features have been found in several positions; the observed He II $\lambda 4686$ -Å line intensity is found to be larger than in galactic WR stars, by a factor of ~ 2 . Exceptionally broad components of permitted lines of hydrogen and helium (FWHM ~ 2500 km s⁻¹) are observed in one of the brightest stars in NGC 604. This object shows a large overabundance of He and strong spectral variability on time-scales of ~ 10 yr. We classify it as an LBV–WR transition object.

We identify the core of the cluster ionizing the nebula, which is probably younger than 5 Myr.

Implications of these results for the evolutionary state of NGC 604 are discussed. Also discussed are the difficulties involved in the techniques for using RSGs as tracers of starburst activity in galactic nuclei.

Key words: techniques: spectroscopic – supergiants – stars: Wolf-Rayet – ISM: abundances – H II regions – ISM: individual: NGC 604.

1 INTRODUCTION

The mass of an ionizing cluster (M_{\star}) in a star-forming complex can be inferred in several ways. An order-of-magnitude estimate results from measuring the number of ionizing photons in the ionized region, which, when related to the

★Present address: Space Telescope Science Institute, 3700 San Martin Drive, Baltimore, MD 21218, USA.

†Present address: VILSPA, IUE Observatory, ESA, Villafranca del Castillo, 28080 Madrid, Spain.

number of required massive stars and to a given initial mass function, provides M_* . Two other methods can be used, both under the assumption of the virial theorem, to infer the total mass enclosed within a certain volume. These involve accurate measurements of the gas velocity dispersion (σ_{gas}) and, although technically more demanding (see below), direct measurements of the stellar velocity dispersion (σ_*) by means of absorption lines like the near-infrared Ca II triplet (CaT). The inferred mass, minus the mass of gas (M_G) within the volume, gives an estimate of M_* .

The measurement of σ_* requires the detection of stellar absorption features in the star-forming complex. Unfortunately, the optical cluster continuum is basically featureless, since the spectra of OB stars dominating the light around $\lambda 3500\text{--}7000\text{ \AA}$ show weak absorption lines that, for clusters younger than about 5 Myr, coincide with the strong emission from the associated H II region (Kinman & Davidson 1981; Rayo, Peimbert & Torres-Peimbert 1982; Melnick, Moles & Terlevich 1985). On the other hand, the IR CaT ($\lambda 8498, 8542, 8662\text{ \AA}$) is the most prominent absorption feature in the infrared spectrum of late-type stars and normal galaxies. At metallicities higher than 0.5 of solar, it is very sensitive to luminosity, its strength increasing with decreasing surface gravity (Díaz, Terlevich & Terlevich 1989, and references therein), and it is seen in a young cluster containing luminous red supergiants that dominate the near-IR light (e.g., NGC 2004: Bica & Alloin 1987). This should occur after about 4.5 Myr of evolution according to recent stellar evolution models (Schaller et al. 1992; Bressan et al. 1993; Charbonnel et al. 1993a, b; Schaerer et al. 1993a, b; Fagotto et al. 1994a, b).

This combination of weak optical absorption lines with strong IR CaT has been found to be the case in one of the circumnuclear H II regions of the nearby starburst galaxy NGC 3310 (Terlevich et al. 1990); the CaT features can also be seen in other circumnuclear regions in the same galaxy (Pastoriza et al. 1993). This result confirms the theoretical predictions by Campbell & Terlevich (1984).

Yet the question of why no CaT detections have been reported in giant extragalactic H II regions (GEHR) still remains unanswered. Reasons for this include the scarcity of high signal-to-noise ratio spectra at wavelengths longer than 7500 \AA , and the strong selection bias towards systems with the strongest emission lines that are excellent candidates for the accurate determination of abundances but are probably too young to host red supergiants. Specifically designed observations are therefore needed in order to assess the presence or absence of CaT features on the spectra of GEHR and their use to measure σ_* . This has been one of the main objectives of a European collaboration for the study of star formation (GEFE).¹ The giant H II region NGC 604 on the disc of the Sc galaxy M33 was chosen as a target, since observations in the *B*, *V* and *R* photometric bands produced colour-magnitude diagrams that seem to indicate the presence of a population of red supergiant stars (Debray 1991).

NGC 604, being the second most luminous H II region in the Local Group (after 30 Dor in the LMC), has been studied extensively. It has a core-halo structure with a total diameter of about 450 pc (Israel & Van der Kruit 1974; Sandage & Tammann 1974), with the most massive stars concentrated to the inner 140 pc (Drissen, Moffat & Shara 1993, hereafter DMS93). The total H β luminosity of the region implies ionization by a star cluster whose energy input is equivalent to that of 100 O6 stars (Melnick 1979). The presence of WR stars in NGC 604 was noted by Conti & Massey (1981, hereafter CM81) and D'Odorico & Rosa (1981), and quantitative studies of their population have been made by Drissen, Moffat & Shara (1990, hereafter DMS90) and DMS93, who give a number ratio of WR to O stars of 0.1. The ionization structure and spatial distribution of abundances in the nebula have been studied by Díaz et al. (1987, hereafter DTPVE87). Internal kinematical information can be found in Rosa & Solf (1984), Clayton (1988) and Sabalisck et al. (1995).

2 OBSERVATIONS AND DATA REDUCTION

Spectroscopic data were obtained with the 4.2-m William Herschel Telescope (WHT) at the Roque de los Muchachos Observatory in La Palma on 1992 October 24 and 25. Blue and red spectra were obtained simultaneously using the ISIS double long-slit spectrograph (Clegg 1991) and two UV coated 1280×1180 CCD detectors. Gratings of 300 and 316 groove mm^{-1} were used, respectively, in the blue and red arms, covering from $\lambda 3700$ to 5500 \AA and from $\lambda 7900$ to 9700 \AA . The dispersion of $1.4\text{ \AA pixel}^{-1}$ with a slit width of 1.2 arcsec gives a spectral resolution of about 4 \AA . The extent of the CCD along the spatial direction was reduced to 3 arcmin , with a sampling of $0.66\text{ arcsec pixel}^{-1}$.

Two different observing techniques were used. On the first night, we scanned manually the core region of NGC 604 by positioning the slit first at PA 60° , displacing it by 1 arcsec and taking a 1-min exposure, and repeating the process until a total area of $1.75 \times 0.23\text{ arcmin}^2$ was covered. The same procedure was followed at PA 120° , covering now $1.75 \times 0.18\text{ arcmin}^2$. Both 'scannings' were centred at RA = $01^{\text{h}}31^{\text{m}}43^{\text{s}}$, Dec. = $30^\circ31'52''$. Fig. 1(b) shows the scanned area, superimposed on a JKT image of the continuum, taken through a redshifted H α narrow filter ($\lambda 6830\text{ \AA}$). An H α emission image with H α continuum contours overlapped is shown in Fig. 1(a).²

Two fixed positions of the slit at PA 293° and 311° , chosen also from the JKT continuum map, were observed on the second night. They are marked in Fig. 1(c). A journal of observations is given in Table 1. Both nights had relatively good seeing (about 1 arcsec).

The blue spectra were reduced using FIGARO data processing software. The procedure, detailed in González-Delgado et al. (1994), includes bias and flat-field corrections, two-dimensional wavelength calibration, corrections for atmospheric extinction and differential refraction and flux calibration. The spatial profile of the sky light distribution was used to flatten the frames in the spatial direction prior to sky subtraction.

²The JKT images belong to the GEFE catalogue of giant extragalactic H II regions.

¹GEFE, Grupo de Estudios de Formación Estelar, is an international collaboration of astronomers from Spain, the UK, France, Germany, Denmark and Italy, formed to take advantage of the international time granted by the Comité Científico Internacional at the Observatories in the Canary Islands.

The near-IR spectra, central to our project, require an extremely careful processing to properly subtract the sky, which has in the region OH emission lines and water vapour atmospheric absorptions so intense that they could be used for wavelength calibration (e.g. Osterbrock & Martel 1992). An example of the sky emission is shown in Fig. 2.

These spectra were reduced following the same steps as the blue ones, but using routines available in the IRAF software package, which allowed better sky subtraction. The two-dimensional scanning performed in each position angle was compressed in the spatial direction and added up to produce an integrated one-dimensional spectrum. For the fixed slit position frames, extraction zones for the one-

dimensional spectra were selected from spatial profiles obtained in the continuum, to maximize the chances of detecting stellar components. Figs 3(a) and (b) show the spatial profile for both slit positions. Arrows indicate the extraction pixels, and the regions are listed in Table 2.

3 RESULTS AND DISCUSSION

3.1 The large-aperture spectrum of NGC 604

Figs 4 and 5 show respectively the blue and far-red spectra corresponding to the scanned region (see Fig. 1b). Both position angles were co-added in order to obtain an inte-

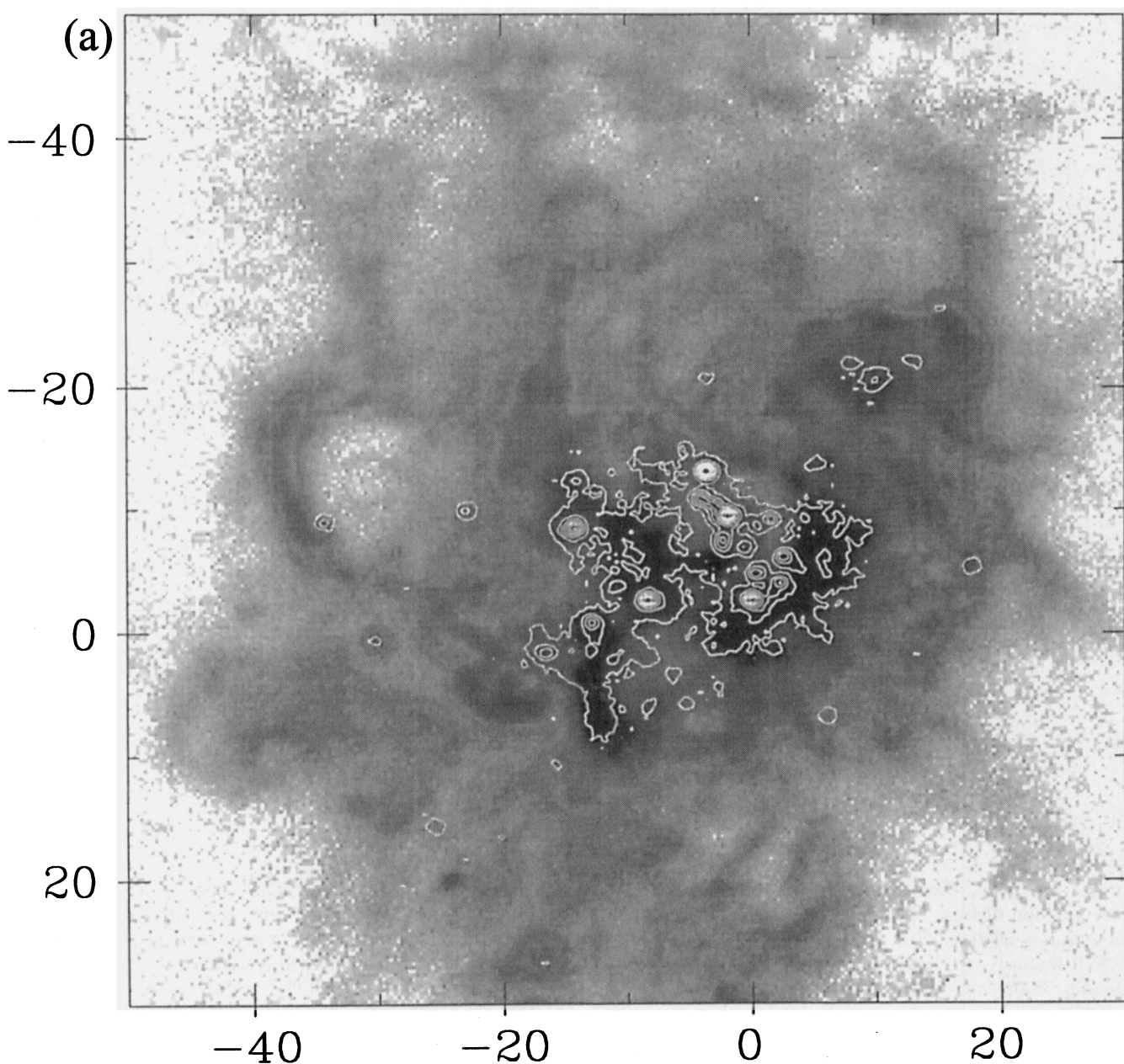
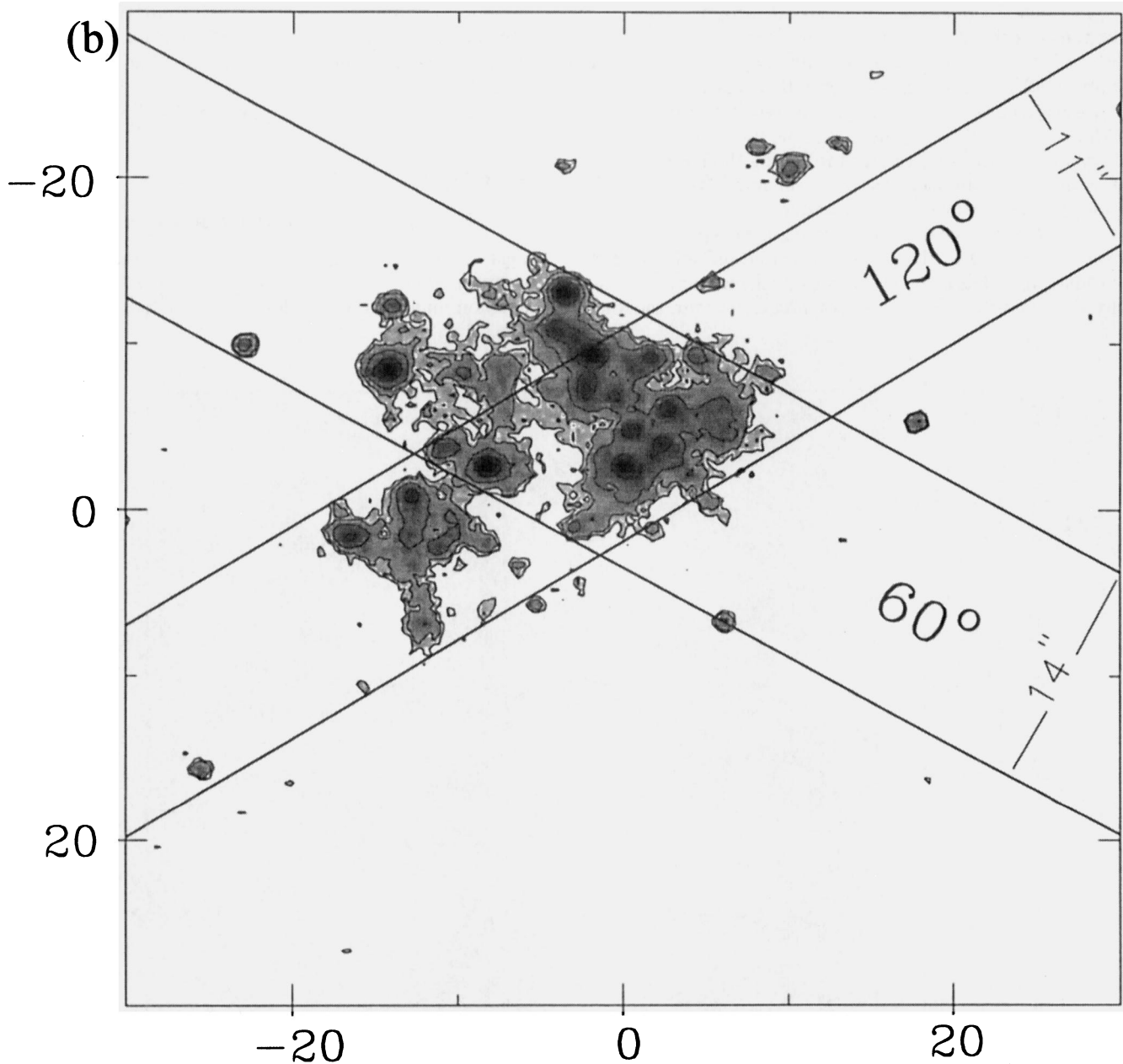


Figure 1. (a) $H\alpha$ emission image, $H\alpha$ continuum contours overlapped. (b) Continuum contours, scanned area overlapped. (c) Continuum contours, slit positions overlapped; regions extracted are identified. North is to the top and east to the left; ticks are in arcsec.

**Figure 1** - *continued*

grated spectrum. Fine details can be appreciated in the insets of the figures. The signal-to-noise ratio in the continuum is ~ 60 at $\lambda 4550 \text{ \AA}$ and ~ 16 at $\lambda 9150 \text{ \AA}$.

WR features are clearly detected in the blue scan, with a double bump corresponding to broad emission at He II $\lambda 4686 \text{ \AA}$ and N III at $\lambda \lambda 4634, 4640, 4642 \text{ \AA}$, characteristic of WN stars. The absence of the N V lines at $\lambda \lambda 4602, 4620 \text{ \AA}$ indicates an intermediate type. The nebular line of [Fe III] $\lambda 4658 \text{ \AA}$ is also present.

The mode in which the scanning was performed precludes an accurate absolute flux calibration solely on the

basis of our observations. The photoelectric photometry data of Searle (1971) have then been used to provide an absolute scale for the integrated flux. According to this calibration the measured H β flux inside a circular aperture 14 arcsec in diameter is $F(\text{H}\beta) = 2.2 \times 10^{-12} \text{ erg cm}^{-2} \text{ s}^{-1}$. This area (154 arcsec^2) happens to be equal to our scanned area ($14 \times 11 \text{ arcsec}^2$). With this calibration, the flux measured in the broad He II feature is $2.7 \times 10^{-13} \text{ erg cm}^{-2} \text{ s}^{-1}$. Assuming a distance to M33 of 720 kpc (Allen 1973) and a constant extinction value through the nebula of $C(\text{H}\beta) = 0.36$ (DTPVE87), the total luminosity of the broad

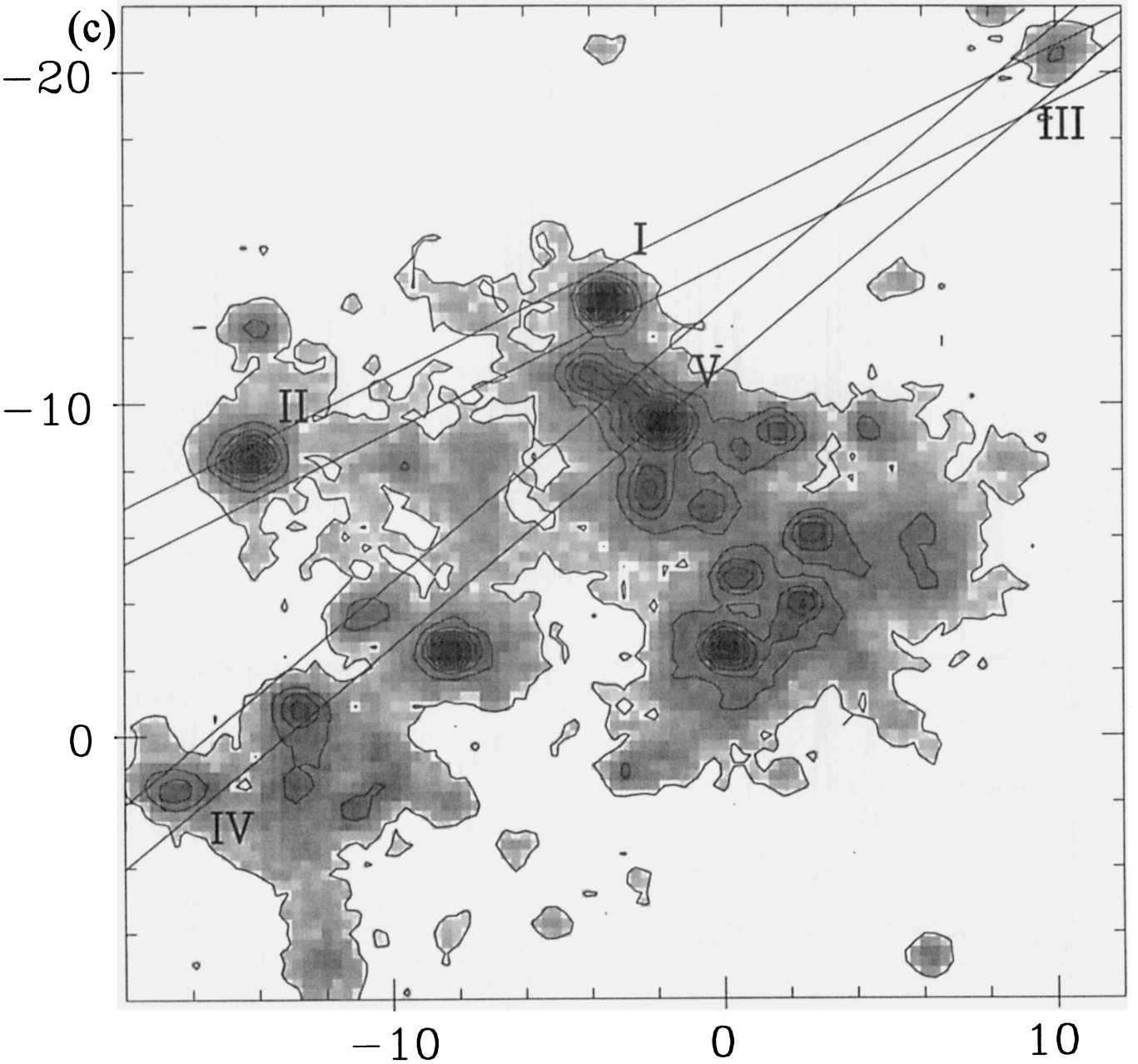


Figure 1 – continued

Table 1. Journal of observations.

Scanned Spectra. Date: 1992 October 24/25.

Grating	$\Delta\lambda$ (Å)	PA	Exposure (s)	Slit width (arcsec)
316R	7900–9700	60	3600	1.0
300B	3700–5500	60	3600	1.0
316R	7900–9700	120	1800	1.0
300B	3700–5500	120	1800	1.0

Fixed Position Spectra. Date: 1992 October 25/26.

Grating	$\Delta\lambda$ (Å)	PA	Exposure (s)	Slit width (arcsec)
316R	7900–9700	293	3600	1.2
300B	3700–5500	293	3600	1.2
316R	7900–9700	311	3600	1.2
300B	3700–5500	311	3600	1.2

He II feature, taking out the contribution of the [Fe III] $\lambda 4658$ -Å line, is $4.3 \times 10^{37} \text{ erg s}^{-1}$. This comprises the broad features of both N III $\lambda\lambda 4634, 4640, 4642$ Å and He II $\lambda 4686$ Å.

Recently measured fluxes of the He II line in WR stars in the LMC are given in Vacca & Conti (1992). The average luminosity per single WNL star is, according to these authors, $1.7 \times 10^{36} \text{ erg s}^{-1}$. The contribution of the N III lines to the WR bump seems to be metallicity-dependent and amounts to anything between 0.15 and 0.5 of the total measured flux (Smith 1991). In our data, this contribution is between 0.4 and 0.6, depending on the deconvolution adopted. This gives an He II line luminosity of $(2.1 \pm 0.5) \times 10^{37} \text{ erg s}^{-1}$ which, using the calibration of

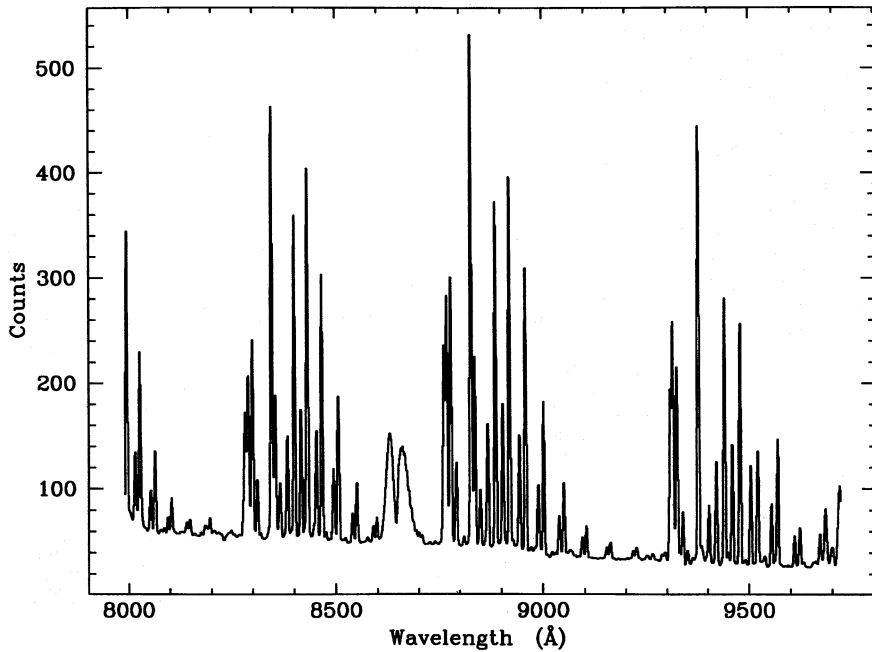


Figure 2. IR sky emission spectrum.

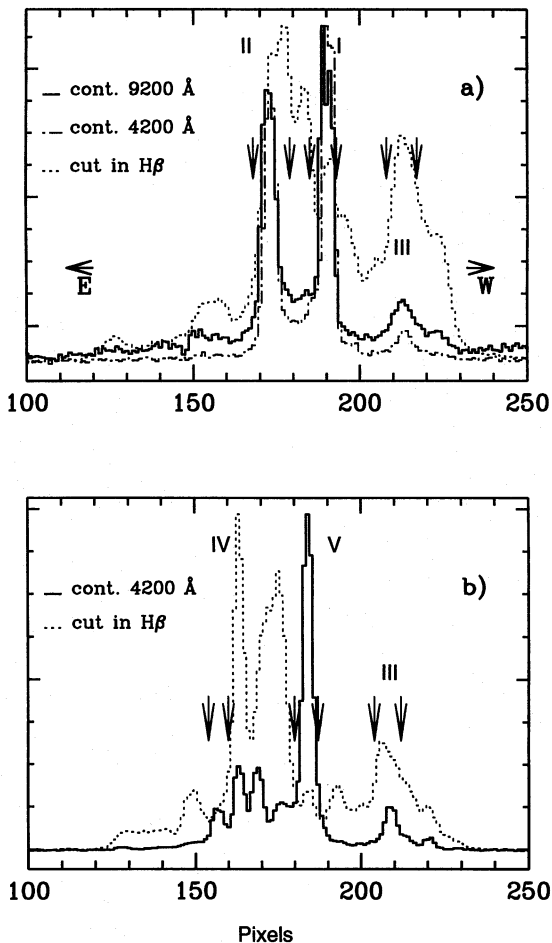


Figure 3. (a) Spatial profiles in continuum light and H β , extractions indicated in PA 293°. (b) The same at PA 311°.

Table 2. One-dimensional extractions.

Region	PA (°)	Pixels
I	293	185–193
II	293	168–179
III	293	208–217
III	311	204–212
IV	311	160–166
V	311	181–187

Vacca & Conti above, suggests about 12 WN stars, in agreement with the 13 WR stars detected with *HST* by DMS93.

Thus the WR stars embedded in NGC 604 show an He II line flux higher than galactic WN stars by a factor of about 2, consistent with earlier suggestions (CM81). Numbers of WR stars derived from measured fluxes of the whole WR bump, i.e., without subtracting the contribution of the N III lines, using galactic WR stars as calibrators may be severely overestimated and should therefore be taken with great caution when using them as constraints for models of stellar and galactic evolution.

The most prominent emission feature in the red scan (Fig. 5) is the Paschen series of hydrogen from P₈ at $\lambda 9546$ Å down to the Paschen discontinuity at $\lambda \approx 8200$ Å. The ratio of this discontinuity to the H β intensity [$I(\text{H}\beta)$] is, after correcting for the adopted extinction of $C(\text{H}\beta) = 0.36$,

$$\frac{\Delta P_a}{I(\text{H}\beta)} = 3.12 \times 10^{-4} \text{ Å}^{-1} = 7 \times 10^{-15} \text{ Hz}^{-1}.$$

According to the models computed by González-Delgado et al. (1994) for the He abundance of $\text{He}^+/\text{H}^+ = 0.075$ derived for NGC 604 (DTPVE87), this $\Delta P_a/I(\text{H}\beta)$ ratio implies an electronic temperature of 8000 K. This value coincides with

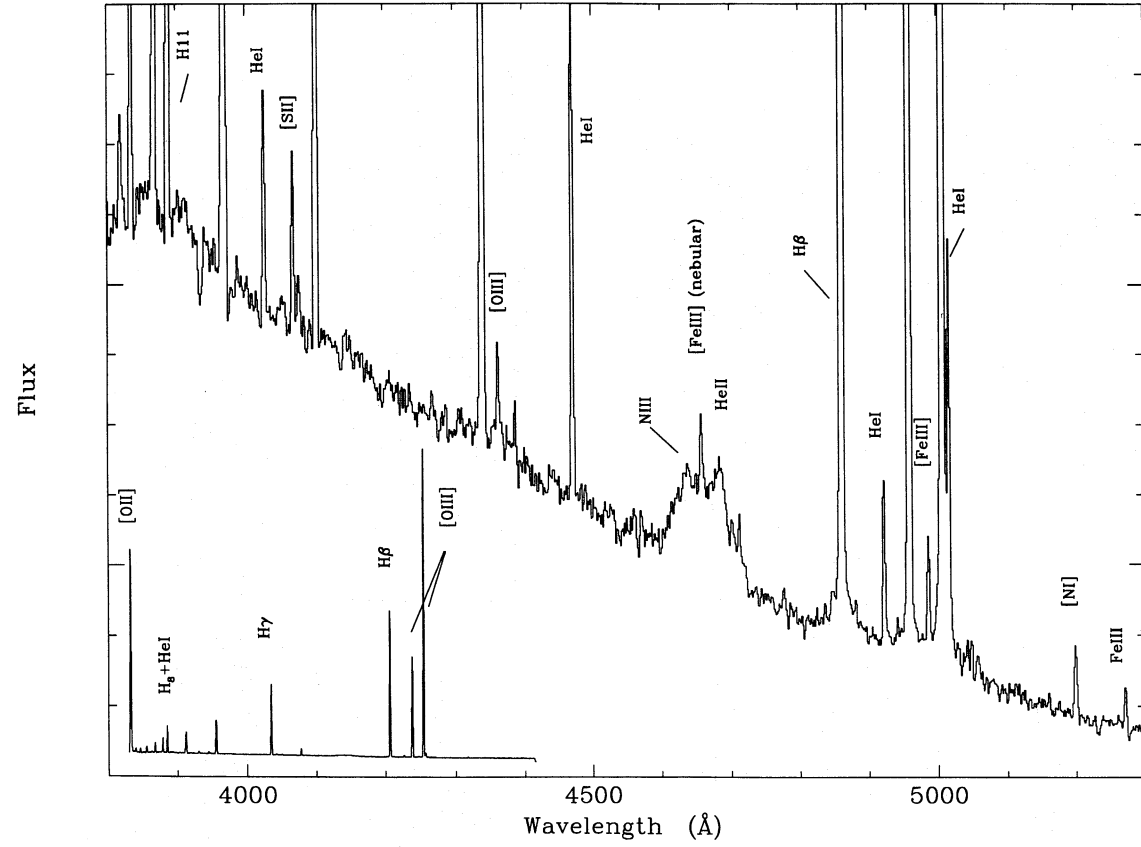


Figure 4. Scan blue combined spectrum in two scales (full spectrum shown in the inset).

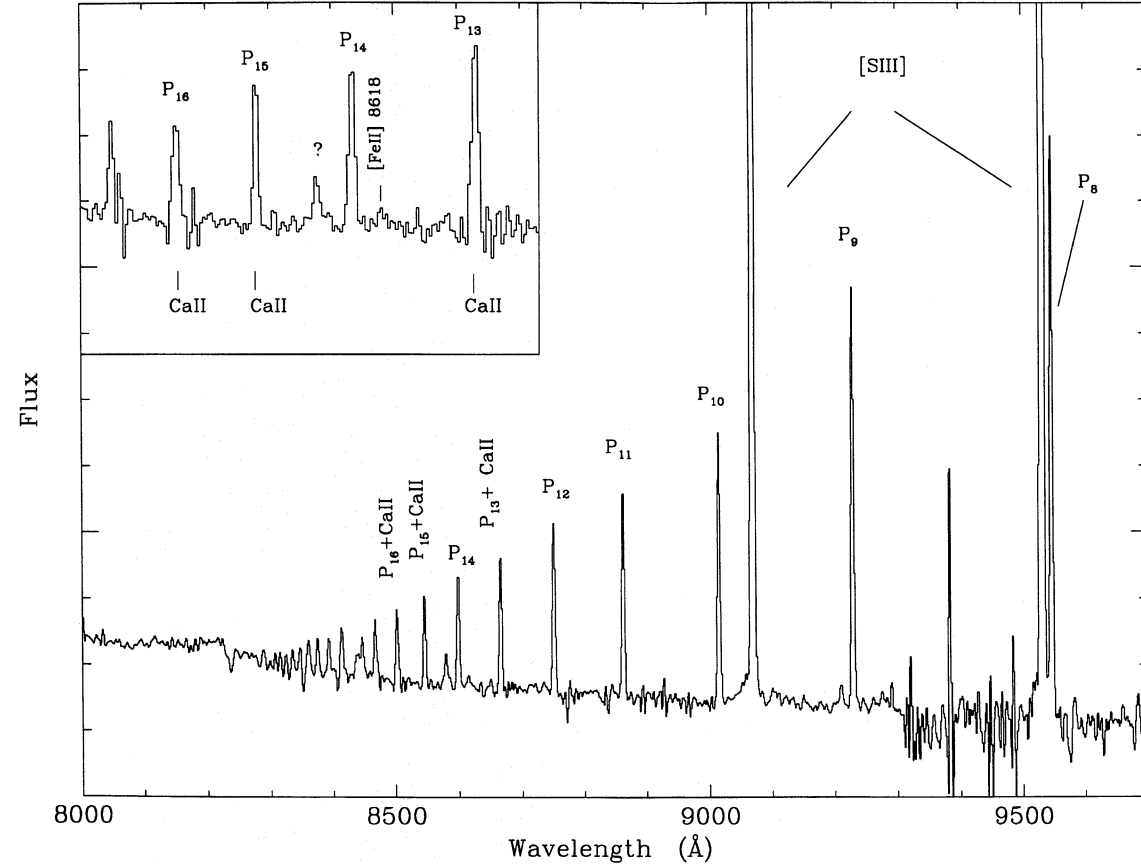


Figure 5. Scan red combined spectrum in two scales (CaT lines position indicated in the inset).

the average temperature found by DTPVE87 from the observed ratio of auroral to nebular [O III] lines for the brightest emission knots. As permitted and forbidden lines are produced in different regions of the nebula, we conclude that no appreciable temperature fluctuations exist in NGC 604.

The strength of the Paschen lines precludes any positive detection of the Ca II absorption lines, since their wavelengths (8498, 8542 and 8662 Å) are very close to those of P₁₆ (8502 Å), P₁₅ (8545 Å) and P₁₃ (8665 Å). None the less, broad absorption wings in the P₁₆, P₁₅ and P₁₃ lines can be

seen by inspection of the inset in Fig. 5, which are not observed in the rest of the Paschen series (e.g., P₁₄). However, attempts to subtract the Paschen emission lines in the way described below (see Section 3.2) were not successful in the integrated spectrum.

3.2 Long-slit spectra

In order to minimize the nebular continuum contamination of the spectra of the continuum sources, we have also

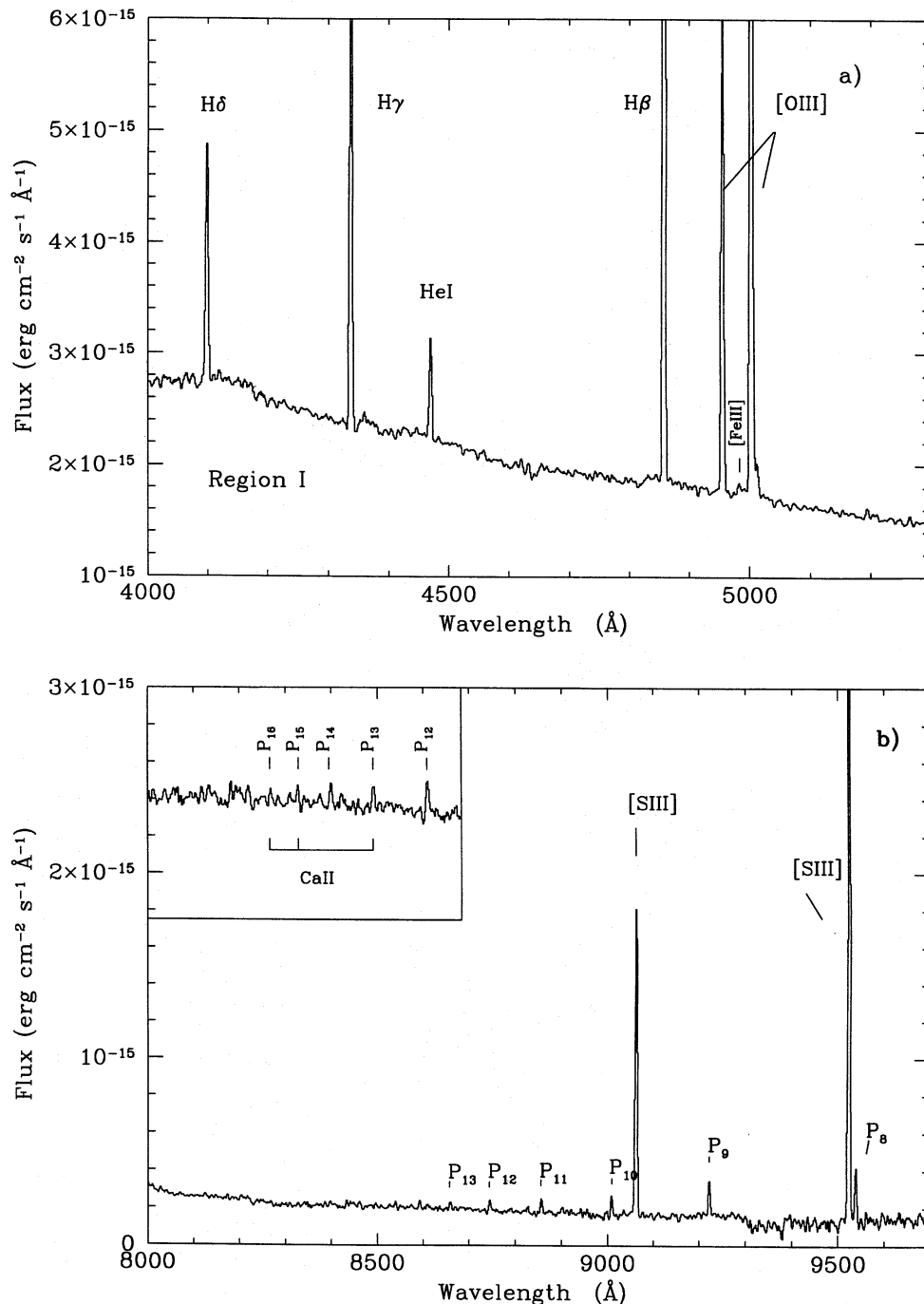


Figure 6. One-dimensional spectra of position I. (a) Blue spectrum; (b) red spectrum with the CaT region shown in the inset.

obtained long-slit spectra at fixed positions. Two slit positions covering most of the strong continuum sources were selected from the JKT CCD images (Fig. 1c). The corresponding position angles are 293° and 311° .

Five different regions have been identified along the slit positions, and their spatial extension in pixels can be seen in Figs 3(a) and (b) (1 pixel=0.66 arcsec). The actual extractions are listed in Table 2. Regions I and II are located on the slit at PA=293°, and regions IV and V at PA=311°. Individual one-dimensional spectra of these regions are

shown in Figs 6–9, with the blue spectra in panels (a) and the corresponding red ones in panels (b). An emission blob labelled III is common to both position angles, and its total spectrum has an exceptionally high signal-to-noise ratio (Fig. 10).

WR features have been detected at positions II, V and IV, and identified with WR stars number 6 and 4 from DMS90 and 11 from DMS93 respectively. Region II also coincides with star CM13 from CM81 and region C from DTPVE87.

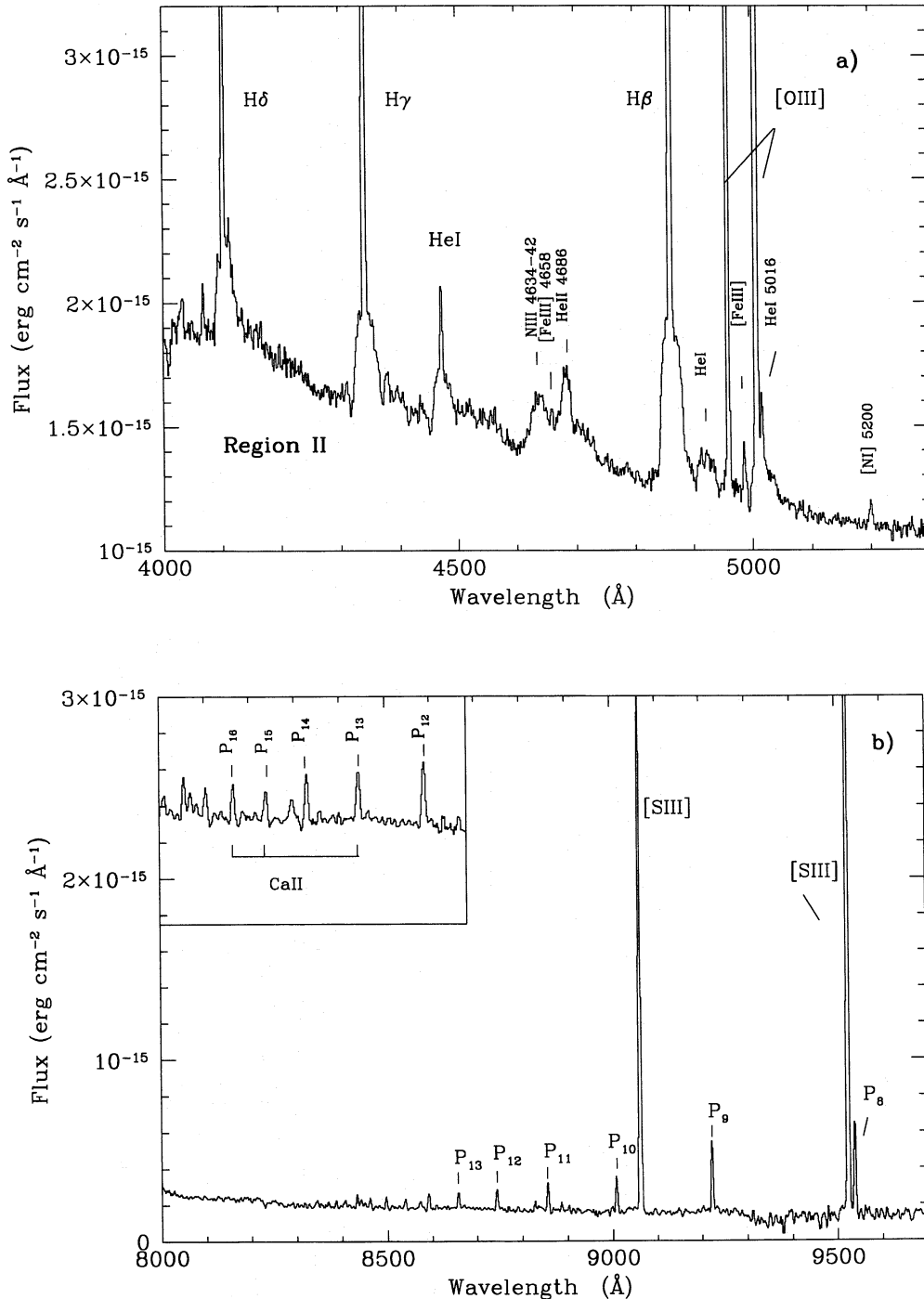


Figure 7. Same as Fig. 6, for position II. WR broad feature is identified in (a); Paschen emission is identified in (b).

3.2.1 Region II: a very luminous broad-emission-line variable object

Our spectrum of this region shows very broad components in the recombination lines of both H and He (see Fig. 7a). However, in the spectrum corresponding to 1984 (DTPVE87), broad components are observed only in the H lines. Further back, the spectrum shown by CM81 has narrow H and He lines and a broad WR feature. This suggests

a strong spectral evolution with the appearance of broad components, first in the H recombination lines and subsequently in the He I ones.

HST images (DMS93) show this object to be a group of four bright stars, with the WR being the easternmost component. A careful analysis of the structure of the two-dimensional spectrum shows a small displacement (fraction of a pixel) of the broad H β component to the east with respect to the continuum source. This is consistent with

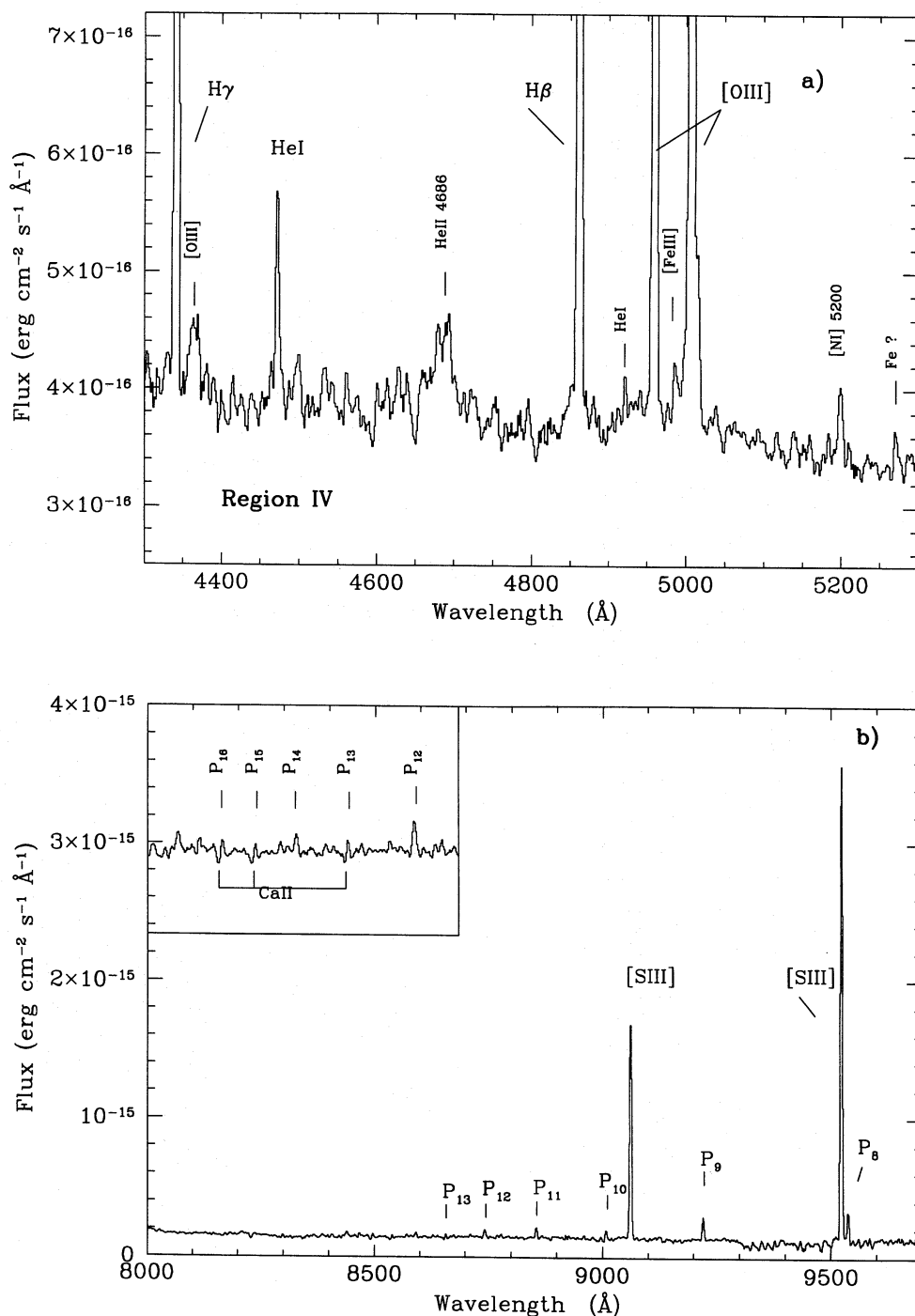


Figure 8. Same as Fig. 6, for position IV. Wings of CaT in absorption can be seen underneath the marked Paschen emission lines.

most of the broad emission in both the H and He lines and the WR features being produced by star W6, while most of the blue continuum is coming from the rest of the cluster. The luminosity of the WR feature is 1.1×10^{36} erg s $^{-1}$, assuming a constant reddening $c(H\beta)=0.36$ (DTPVE87) and a distance of 720 kpc. This is consistent with a single WR star.

We have measured the widths of the broad component of H α and He I $\lambda 6678$ -Å lines from high-resolution (0.37 Å

pixel $^{-1}$) spectra obtained with the WHT and the ISIS spectrograph by the GEFE collaboration (Fig. 11: Mas Hesse et al., private communication). A Gaussian fitting procedure gives a FWHM of 2200 km s $^{-1}$ for both lines (Fig. 12). A straight measurement of the FWHM of the H α broad component gives a somewhat higher value of 2500 km s $^{-1}$.

The measured He I $\lambda 6678$ Å to H α flux ratio is $\approx 0.17 \pm 0.04$, which is larger than the expected ratio of recombination lines for a gas of solar composition (0.01:

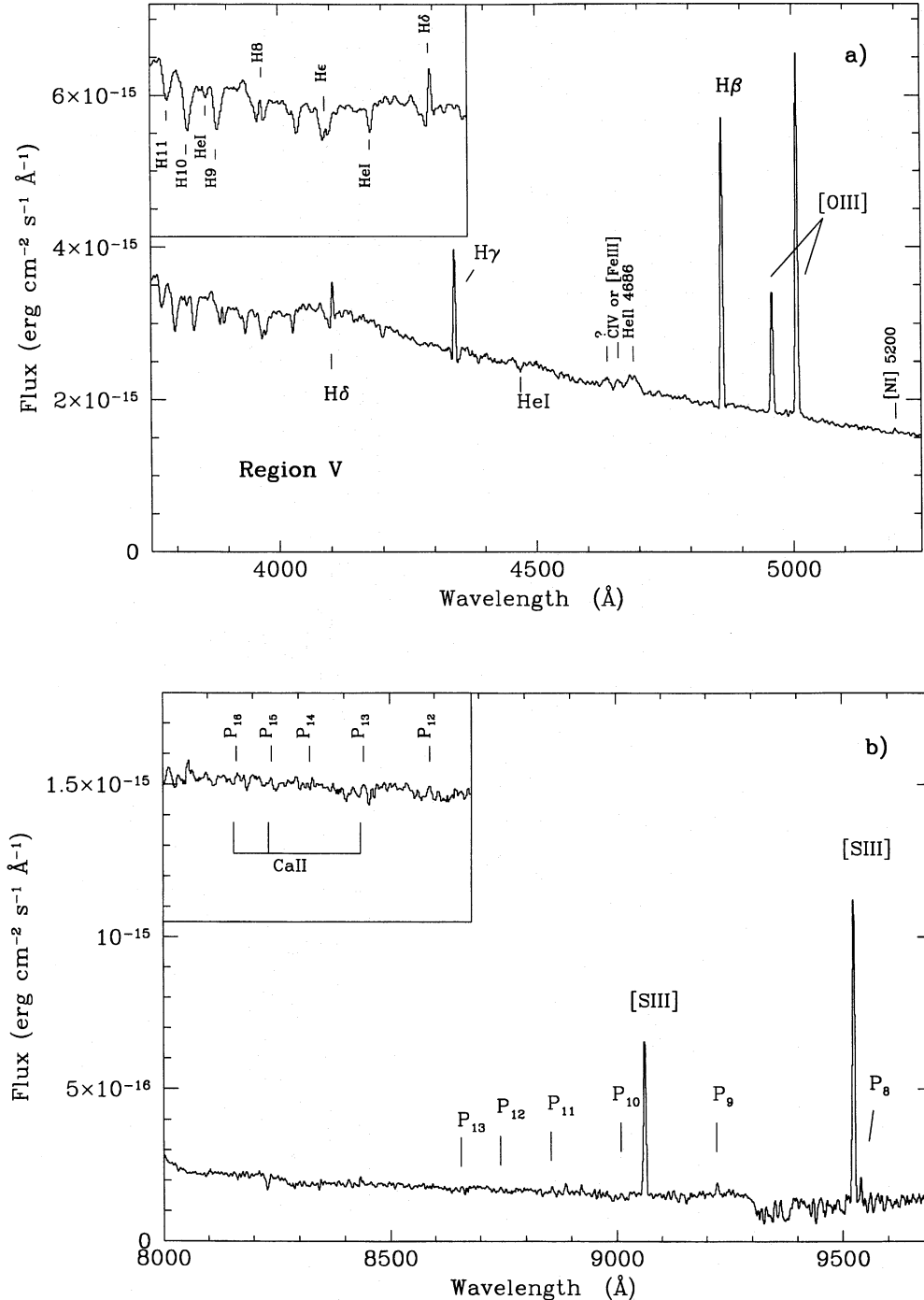


Figure 9. Same as Fig. 6, for position V. Stellar absorptions can be seen in the blue (a); no CaT can be seen in (b).

Osterbrock 1989), yielding a helium abundance $N_{\text{He}}/N_{\text{p}}=1.25$, or a helium enrichment by a factor of about 15 with respect to the solar value.

The observed variability of this object, together with the helium overabundance and the exceptionally large width of the recombination lines suggest that we are observing a transition object between a WR and a luminous blue variable (LBV). This is supported by a hint of P Cygni profiles

in the He I lines and the presence of the [Fe III] lines sometimes observed in the spectra of LBV stars (DMS90). Note that Clayton (1988) detected a rapidly expanding small shell associated with the star. Spectral monitoring of this object will be of great importance.

The red spectrum (Fig. 7b) is relatively noisy, with the Paschen series and the [S III] lines as the most relevant features. No CaT lines are detected.

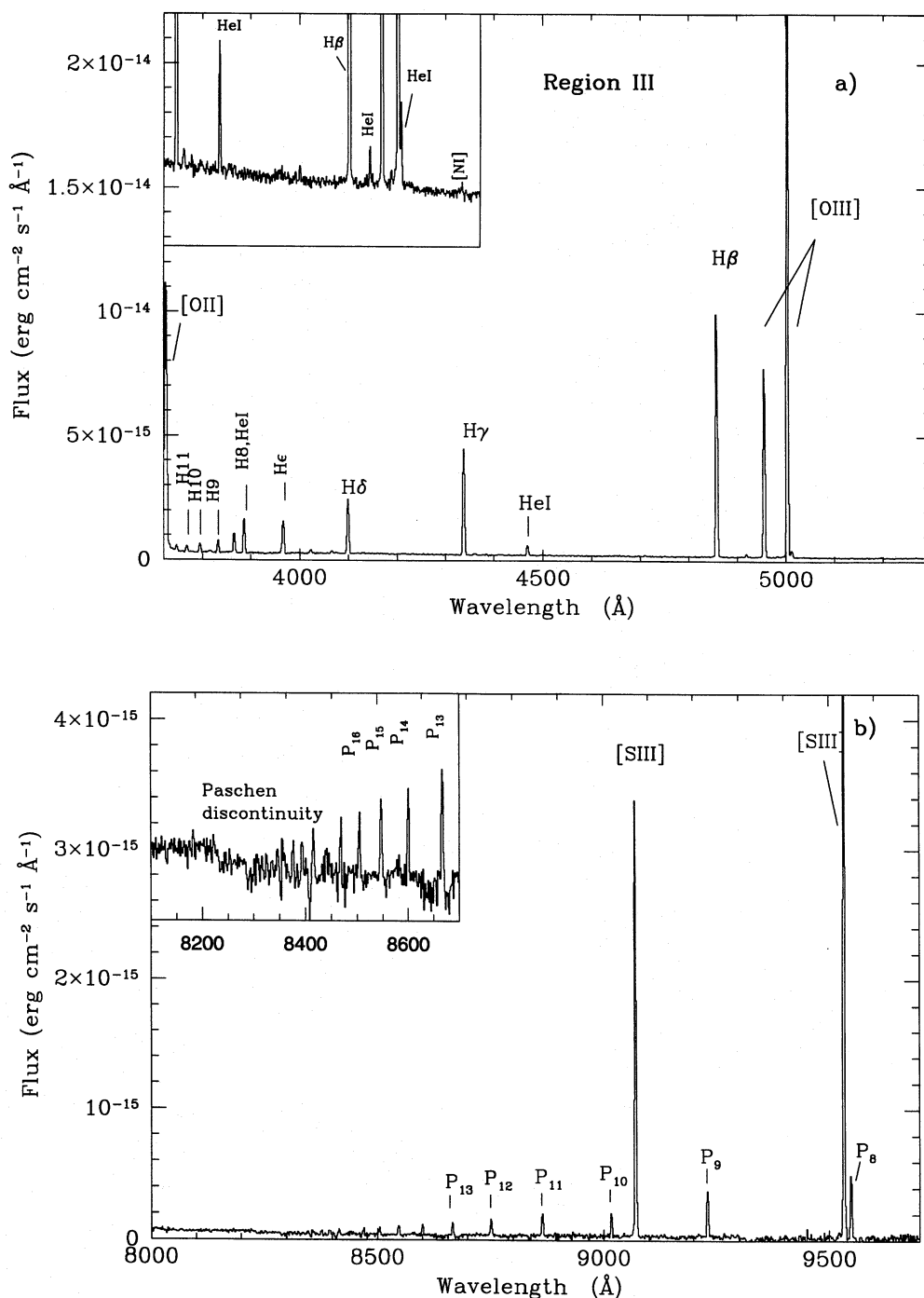


Figure 10. Same as Fig. 6, for position III; the Paschen discontinuity can be seen in the inset of (b).

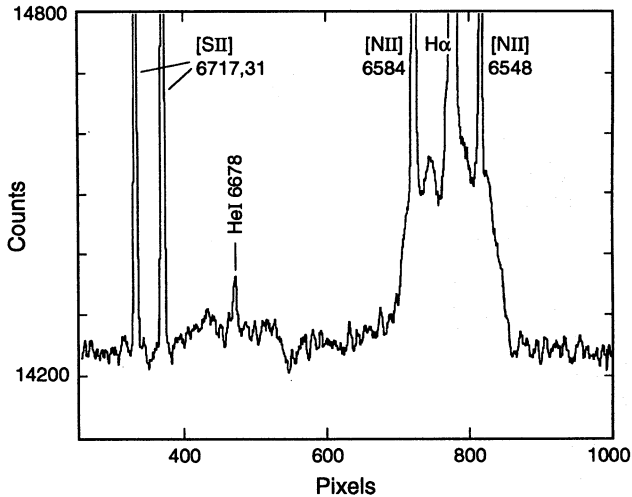


Figure 11. High-dispersion H α and He I λ 6678-Å lines for position II (Mas Hesse et al., private communication).

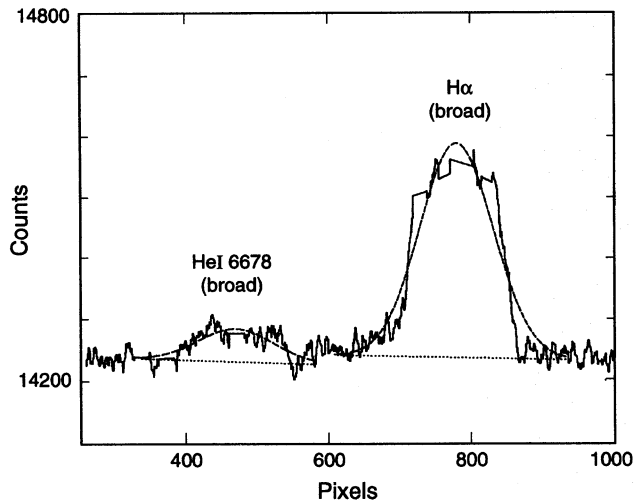


Figure 12. Gaussian fitting to the broad components of the spectrum shown in Fig. 11.

3.2.2 Region IV: the detection of CaT

The spectrum observed at position IV shows a weak WR feature (Fig. 8a). The luminosity of the whole He II ‘bump’ is $3.7 \times 10^{35} \text{ erg s}^{-1}$ which, according to the numbers given in Section 3.1, is, though weak, consistent with a single WR. By comparing our continuum image (Fig. 1) with the blue CFHT image from DMS93 (their fig. 5) we have identified the object at position IV with their star W11.

The red spectrum (Fig. 8b) shows weak Paschen lines in emission with P₁₆, P₁₅ and P₁₃ showing blue absorption wings. The high signal-to-noise ratio emission spectrum from position III has been used as a template to subtract the Paschen series. The resulting spectrum reveals the CaT stellar lines (Fig. 13).

The CaT is diluted by the contribution to the continuum by the blue stars present. The intrinsic equivalent width of Ca II may be higher than the measured value by a factor as

large as 2. The estimated equivalent width of the three lines taken together is 5.7 Å, and the sum of the two strongest ones ($\lambda\lambda$ 8542, 8662) is 4.6 Å, consistent with it being produced by RSG stars at the metallicity of NGC 604 (Díaz et al. 1989). Careful measurements of the position of our observed object compared with the *HST* images suggest that the RSG star could be either their star # 109 or # 112. Their absolute blue magnitudes are very similar: -4.15 and -4.05 . This is 2 mag fainter than the absolute blue magnitude of the brightest RSG observed in star-forming regions (Wilson & Matthews 1995). Therefore, if the observed CaT originated in an RSG, it should be of class Iab with a mass of about $13 M_{\odot}$, much older than the rest of the cluster. However, we found no other evidence for previous star-forming episodes in NGC 604.

A second possibility is that the CaT belongs to a galactic foreground dwarf star. In that case, the star would be placed at a distance of about 10 kpc from the Sun. However, halo dwarfs have CaT strengths which are substantially smaller than that measured in this star (Díaz et al. 1989).

Alternatively, we might be observing a region of locally enhanced obscuration. This is supported by the fact that the WR star found in this region (W11) is abnormally faint ($M_B = -2.84$) as compared to the rest of WR stars observed ($M_B \leq -4.79$). It is also supported by the colours of the continuum, which are redder than those observed in the rest of the regions. Therefore both the RSG and the WR stars are consistent with having high-mass progenitors ($m \sim 40 M_{\odot}$) if there are 2 mag of extra extinction in the blue, in agreement with the observed continuum colours. This is our adopted option.

The fact that we see WR and RSG features at the same location (position IV) implies that we are indeed observing a subgroup of young stars in NGC 604. This is consistent with the *HST* images that show a tight group at that position. The members of this group according to the star chart given in DMS93 are stars: # 109, 112, 115, 121, 122 (W11) and 123. The total absolute blue magnitude of the group is -5.7 (-7.7 if 2 mag of extinction are assumed). Note that, by counting stars, M_B could be underestimated.

Theoretical stellar evolution models (Cervino & Mas Hesse 1994; García Vargas, Bressan & Díaz 1995) show that WR and RSG stars in a coeval population coexist only during a short period of time that depends on metallicity. For the abundances of NGC 604 (~ 0.4 solar) this period is between the ages of 4 and 5 Myr.

The relative numbers of stars with masses greater than $20 M_{\odot}$ (O stars), WR stars and RSG stars are, according to the latter models, 1000:43:8, and the observed relative numbers O:WR:RSG are 79:13:1 (DMS93 and this work). Therefore the discrepancy between model and observed WR/O ratios, 0.05 and 0.15 respectively, is a factor of 3 and is not necessarily due to problems with the models; it could probably be attributed to underestimations in the derived numbers of O stars. In fact, from our observed H β luminosity and the radio continuum one (Sramek & Weedman 1986) the required number of ionizing stars is at least twice as large as those inferred from the photometry of DMS93. This is well inside the uncertainties associated with the derivation of masses of young stars from broad-band photometry. To solve this problem, spectroscopic observations of individual stars in NGC 604 are needed.

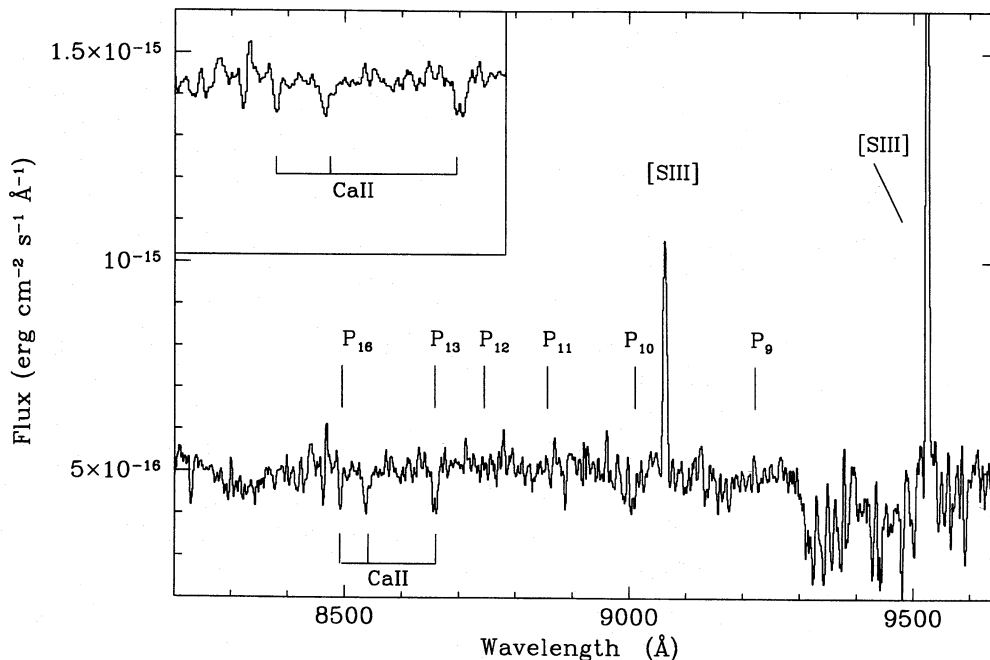


Figure 13. One-dimensional far-red spectrum of position IV, emission template subtracted. CaT in absorption is indicated.

3.2.3 Region V: absorption lines in the blue spectrum

The blue spectrum corresponding to position V (Fig. 9a) also shows WR features and several absorption lines of stellar origin. The absorption lines correspond mainly to He I and H I. Nebular emission is seen in the Balmer lines from H₈ to H β . The measured m_{4400} is 16.0, corresponding to $M_{4400} = -8.2$. Taking into account the average extinction in NGC 604, this value implies $M_B \simeq -9$. Absolute blue magnitudes for the brightest individual stars in DMS93 are around -8 . The type of spectrum and the derived luminosity imply that we are seeing a composite object that probably corresponds to the core of the stellar cluster in NGC 604.

The luminosity of the WR bump (1.4×10^{36} erg s $^{-1}$) can be attributed to one star. The detection of He II $\lambda\lambda 4686$ Å, N III $\lambda\lambda 4634, 4640, 4642$ Å and the non-detection of N V $\lambda\lambda 4604, 4620$ Å suggest that the WR stars are of type late N or intermediate.

The red spectrum shows weak Paschen emission and strong [S III] lines. No CaT lines are detected, consistent with a cluster with an age of less than 5 Myr.

3.2.4 Region III: a pure emission filament

The spectrum extracted from position III represents a pure emission filament (Figs 10a and b). This spectrum, adequately scaled, was used to subtract the Paschen emission from position IV, as discussed above. The Paschen discontinuity is clearly seen, and the reddening-corrected ratio, $\Delta P_{\lambda}/I(H\beta) = 2.7 \times 10^{-4} \text{ Å}^{-1} = 6.1 \times 10^{-15} \text{ Hz}^{-1}$, yields an electron temperature of 10000 K, similar to the value obtained for the highest excitation knots in NGC 604 (DTPVE87) from the forbidden line ratios. This result confirms our conclusion from the scanned spectrum analysis

that no appreciable temperature fluctuations exist in NGC 604.

3.2.5 Region I

Finally, position I, shown for completeness in Figs 6(a) and (b), does not provide much additional information.

4 SUMMARY AND CONCLUSIONS

With the aim of obtaining global spectroscopic information of a nearby giant H II region, we have obtained high signal-to-noise ratio integrated spectra scanning the central $11 \times 14 \text{ arcsec}^2$ region in NGC 604 with the WHT and the double spectrograph ISIS. The presence of a strong Paschen series in emission in the red scan precludes the detection of the absorption lines of the stellar luminosity indicator Ca II triplet, which is very close (in wavelength) to P₁₆, P₁₅ and P₁₃. The Paschen discontinuity at $\lambda \simeq 8200$ Å is clearly detected, and its ratio to the intensity of H β allows us to determine a $T_e \sim 8000$ K, similar to the one obtained by DTPVE87 from [O III] forbidden line ratios; this result suggests that no temperature fluctuations are present in the nebula. The WR features detected in the blue spectral region imply the presence of 12 WN stars, using the calibration for LMC WR stars given in Vacca & Conti (1992). This is in excellent agreement with the 13 WR stars derived from HST images taken with a $\lambda 4686$ -Å narrow-band filter (DMS93). If one were to adopt the standard calibration for galactic WR stars from Kunth & Sargent (1981), a larger number (21) would be deduced. This indicates that the WR stars in NGC 604 have a higher He II $\lambda 4686$ -Å luminosity than the galactic ones, as already suggested by CM81.

We have selected objects with strong red continuum from a narrow-band JKT image, to maximize the chance of

detecting the CaT absorptions. Two position angles for long-slit observations were chosen ($PA = 293^\circ$ and 311°) so as to cover several of them simultaneously. Five different regions, identified along the slit positions, were extracted as positions I to V. WR features, present in regions II and V, show intensities consistent with them being produced by a single star in each case, and have been identified with WR stars 6 and 4 from DMS90. A fairly weak He II bump is detected in position IV, identified with the abnormally weak WR star #11 from DMS93. This, together with the red continuum colours, leads us to believe that there might be 2 mag of localized extinction in that region.

A peculiar object in position II that coincides with CM13 from CM81, and with region C from DTPVE87, shows spectral variability, He overabundance, and exceptionally broad recombination lines, a hint of P Cygni profiles in the He I lines and [Fe III] emission; we have tentatively classified it as a transition object between LBV and WR.

Clear evidence for absorption wings corresponding to the CaT was detected only in region IV. Subtracting the pure emission, high signal-to-noise ratio spectrum obtained from position III reveals the stellar feature with strength consistent with one RSG. We cannot therefore determine stellar velocity dispersions from these observations. The fact that we see a WR and an RSG star in the same location suggests that we are observing a subgroup of young stars in NGC 604 of ages between 4 and 5 Myr, according to present stellar evolution models.

A composite stellar population spectrum is observed in the bright region V, a position that we identify with the core of the cluster in NGC 604. High-dispersion ($\sim 6 \text{ km s}^{-1}$ resolution) observations covering the spectral region $3700\text{--}4800 \text{ \AA}$ may allow us to measure the stellar velocity dispersion through OB stars absorption lines like He I $\lambda 4026 \text{ \AA}$, Si IV $\lambda 4089 \text{ \AA}$, Si III $\lambda 4552 \text{ \AA}$, O II $\lambda 4649 \text{ \AA}$ and C III $\lambda 4650 \text{ \AA}$.

A comparison of the electron temperature deduced from the Paschen discontinuity to $I(H\beta)$ ratio measured in the emission region III allows us to confirm the result obtained from the integrated spectra, namely that no electron temperature fluctuations are present in the nebula.

We set out to measure the stellar velocity dispersion in a giant region of star formation using the CaT lines; however, we found no strong CaT in NGC 604. This is the same result found in other regions of star formation that we have analysed (GEFE collaboration, in preparation). The only detections of the CaT in the integrated spectra of star-forming regions remain those of the circumnuclear regions in NGC 3310 (Pastoriza et al. 1993).

Our general conclusion is that the results in NGC 604 are consistent with the theoretical predictions. The CaT should be very weak in a stellar cluster younger than 10 Myr (turn-off mass larger than $20 M_\odot$) and therefore still capable of ionizing the gas, producing an H II region. This is valid only for clusters with small age spread. Regions with large age spread or with two or more different stellar populations can combine the strong CaT characteristic of stars with ages between 8 and 20 Myr with features that are present at other times, such as strong WR bumps (ages between 3 and 8 Myr) or redder continuum and weaker CaT (ages larger than 40 Myr). The circumnuclear H II regions in NGC 3310 may represent examples of mixed populations where the

CaT is not associated with the present burst, but originated instead in an underlying older population. The fact that we find a trend between the equivalent width of $H\beta$ ($W(H\beta)$) and the strength of the CaT, in the sense that those regions with large $W(H\beta)$ have the weakest CaT, supports the mixed population scenario.

We conclude by pointing out an obvious result, relevant for stellar population studies in starbursts and galactic nuclei. The detection of strong CaT in absorption implies the presence of young massive stars. The opposite, nevertheless, is not true: the absence of CaT does not necessarily mean the absence of massive stars.

ACKNOWLEDGMENTS

We are grateful to the Comité Científico Internacional for allocating 5 per cent of the Observatory time during 18 months to the GEFE collaboration. The 4.2-m William Herschel Telescope is operated by the Royal Greenwich Observatory at the Spanish Observatorio del Roque de los Muchachos of the Instituto de Astrofísica de Canarias. We acknowledge the use of the Starlink Software Collection of the UK Particle Physics and Astronomy Research Council for calibration of the data presented in this paper. This work has been partly financed by DGICYT grant PB91-0531 (GEFE), grants for collaborative research (Acciones Integradas British Council-DGICYT and NATO CRG 920198) and EEC network (ANTARES). EP is grateful to the IAC for support during the realization of this work, and ET thanks RGO for its hospitality. We benefited from fruitful discussions with Peter Conti, Bill Vacca and Guillermo Tenorio-Tagle, and from Jorge Melnick's comments which greatly improved the clarity of the paper. We thank Richard Sword for producing Figs 11 and 12. Above all, we are grateful to our collaborators in GEFE, for providing excellent narrow-band JKT images and WHT high-resolution spectra prior to publication, and for generating a cheerful atmosphere that makes working in this group a truly enjoyable experience.

REFERENCES

- Allen C. W., 1973, *Astrophysical Quantities*, 3rd edn. Athlone Press, London, p. 287
- Bica E., Alloin D. M., 1987, *A&A*, 186, 49
- Bressan A., Fagotto F., Bertelli G., Chiosi C., 1993, *A&AS*, 100, 647
- Campbell A. W., Terlevich R., 1984, *MNRAS*, 211, 15
- Cerviño M., Mas Hesse M., 1994, *A&A*, 284, 749
- Charbonnel C., Meynet G., Maeder A., Schaller G., Schaerer D., 1993a, *A&AS*, 101, 415
- Charbonnel C., Meynet G., Maeder A., Schaller G., Schaerer D., 1993b, *A&A*, 279, 338
- Clayton C. A., 1988, *MNRAS*, 231, 191
- Clegg R. E. S., 1991, *Gemini*, 31, 8
- Conti P. S., Massey P., 1981, *ApJ*, 249, 471 (CM81)
- Debray B., 1991, in van der Hucht K. A., Hidayat B., eds, *Proc. IAU Symp. 143, Wolf-Rayet Stars and Interrelations with other Massive Stars in Galaxies*. Kluwer, Dordrecht, p. 427
- Díaz A. I., Terlevich E., Pagel B. E. J., Vilchez J. M., Edmunds M. G., 1987, *MNRAS*, 226, 19 (DTPVE87)
- Díaz A. I., Terlevich E., Terlevich R., 1989, *MNRAS*, 239, 325
- D'Odorico S., Rosa M., 1981, *ApJ*, 248, 1015

- Drissen L., Moffat A. F. J., Shara M. M., 1990, *ApJ*, 364, 496 (DMS90)
- Drissen L., Moffat A. F. J., Shara M. M., 1993, *AJ*, 105, 1400 (DMS93)
- Fagotto F., Bressan A., Bertelli G., Chiosi C., 1994a, *A&AS*, 104, 365
- Fagotto F., Bressan A., Bertelli G., Chiosi C., 1994b, *A&AS*, 105, 29
- García Vargas M. L., Bressan A., Díaz A. I., 1995, *A&AS*, 112, 13
- González-Delgado R. M. et al., 1994, *ApJ*, 437, 239
- Israel F., Van der Kruit P., 1974, *A&A*, 32, 363
- Kinman T. D., Davidson K., 1981, *ApJ*, 243, 127
- Kunth D., Sargent W. L. W., 1981, *A&A*, 101, L5
- Melnick J., 1979, *ApJ*, 228, 112
- Melnick J., Moles M., Terlevich R., 1985, *A&A*, 149, L24
- Osterbrock D. E., 1989, *Astrophysics of Gaseous Nebulae and Active Galactic Nuclei*. University Science Books, Mill Valley, CA
- Osterbrock D. E., Martel A., 1992, *PASP*, 104, 76
- Pastoriza M. G., Dottori H. A., Terlevich E., Terlevich R., Díaz A. I., 1993, *MNRAS*, 260, 177
- Rayo J. F., Peimbert M., Torres-Peimbert S., 1982, *ApJ*, 255, 1
- Rosa M., Solf J., 1984, *A&A*, 130, 29
- Sabalitsck N. S. P., Tenorio-Tagle G., Castañeda H. O., Muñoz-Tuñón C., 1995, *ApJ*, 444, 200
- Sandage A., Tammann G., 1974, *ApJ*, 190, 525
- Schaerer D., Meynet G., Maeder A., Schaller G., 1993a, *A&AS*, 98, 523
- Schaerer D., Charbonnel C., Meynet G., Maeder A., Schaller G., 1993b, *A&A*, 280, 346
- Schaller G., Schaerer D., Meynet G., Maeder A., 1992, *A&AS*, 96, 269
- Searle L., 1971, *ApJ*, 168, 327
- Smith L. F., 1991, in van der Hucht K. A., Hidayat B., eds, *Proc. IAU Symp. 143, Wolf-Rayet Stars and Interrelations with Other Massive Stars in Galaxies*. Kluwer, Dordrecht, p. 601
- Sramek P. A., Weedman D. W., 1986, *ApJ*, 302, 640
- Terlevich E., Díaz A. I., Pastoriza M. G., Terlevich R., Dottori H., 1990, *MNRAS*, 242, 48p
- Vacca W. D., Conti P. S., 1992, *ApJ*, 401, 543
- Wilson C. D., Matthews B. C., 1995, *ApJ*, 455, 125